



Research Article

Indentation-based characterization of creep and hardness behavior of magnesium carbon nanotube nanocomposites at room temperature

J. Thornby¹ · D. Verma² · R. Cochrane³ · A. Westwood³ · V. B. Manakari⁴ · M. Gupta⁴ · M. Haghshenas⁵

© Springer Nature Switzerland AG 2019

Abstract

The time-dependent plastic deformation response of magnesium/carbon nanotube (CNT) nanocomposites containing 0.25, 0.5, and 0.75 vol% of carbon nanotubes is investigated through depth nanoindentation tests against monolithic pure magnesium in the present study. The Mg-CNT nanocomposite materials were successfully synthesized via a powder metallurgy technique coupled with microwave sintering followed by hot extrusion to produce 8-mm diameter, long solid bars. All depth-sensing indentation creep tests were conducted at ambient (room) temperature employing a diamond Berkovich pyramidal indenter. These tests are dual-stage, i.e., loading to a prescribed peak load of 50 mN, holding the peak load constant for a dwell period of 500 s, and finally unloading. Various strain rates of 0.01, 0.1, 1, and 10 s⁻¹ were performed to assess the effects of strain rate and dwell time on the ambient temperature creep response of the Mg-CNT nanocomposites. The outcomes of these tests are explained through material hardness, microstructure, the extent of CNT content in each material, and strain rate sensitivity. Upon analyzing the nanoindentation creep tests, the dominant creep mechanism at room temperature was found to be a dislocation creep mechanism. It is also found that CNTs increase the creep resistance of magnesium. Findings of this study can be used as a starting point for a high-temperature creep study on Mg-CNT nanocomposites. This paper is a continued study from our group on time-dependent plastic deformation of Mg nanocomposites (i.e., see Haghshenas et al., *Journal of Composite Materials*, <https://doi.org/10.1177/0021998318808358>). The short-term goal is to provide a compressive picture of the controlling creep mechanisms and their dependency upon, time, temperature, strain rate, volume fraction of the nanoparticles, and the type of the nanoparticles. Mg, in general, is a notorious material for high-temperature application; therefore, the long-term objective is to propose Mg nanocomposite as reliable replacements for Mg when lightweight and creep resistance are needed. However, to be able to confidently suggest such a replacement detailed understanding on the controlling phenomena, mention as short-term goals, are required.

Keywords Mg-CNT nanocomposite · Depth-sensing indentation · Time-dependent plastic deformation · Dislocation creep · Hardness

1 Introduction

Much attraction is drawn to magnesium (Mg) for its abundance, low density, biocompatibility, high damping capacity, great electromagnetic shielding, and the fact that it

is the most easily machinable metal of all structural metals [1]. This makes magnesium the ideal choice not only for automobiles and airplanes, but also for biomedical implants, vibration and noise control systems, sporting equipment, consumer electronics, and other lightweight

✉ M. Haghshenas, meysam.haghshenas@engr.und.edu | ¹Department of Chemical Engineering, University of North Dakota, Grand Forks, USA. ²Nanoscience Instruments, Phoenix, AZ 85044, USA. ³School of Chemical and Process Engineering, University of Leeds, Leeds, England, UK. ⁴Department of Mechanical Engineering, National University of Singapore, Singapore, Singapore. ⁵Department of Mechanical Engineering, University of North Dakota, Grand Forks, USA.



SN Applied Sciences (2019) 1:695 | <https://doi.org/10.1007/s42452-019-0696-9>

Received: 20 January 2019 / Accepted: 30 May 2019 / Published online: 10 June 2019

engineering applications [2, 3]. Despite these merits, magnesium and its alloys have poor abrasion and corrosion resistance, and like any hexagonal-close packed (HCP) metal, magnesium displays notoriously strong anisotropic mechanical properties of limited strength and poor ductility at room temperature which greatly hinders the metal's potential applications [4, 5]. Along these, the greatest drawback that limits Mg and its alloys from the broader application in the automotive and aerospace industries is low creep resistance at elevated temperatures, i.e., above 175 °C, since some critical components operate at and above this temperature [6]. This drawback is attributed to the limited number of slip systems (HCP structure), which makes the metal brittle and susceptible to creep damage [7].

The limitations of magnesium have been successfully circumvented by the development of new magnesium alloys and the addition of reinforcements, i.e., carbon nanotubes (CNTs), alumina (Al_2O_3), carborundum (SiC), silica (SiO_2), and yttria (Y_2O_3) to create magnesium composites [8, 9]. Specifically, metal matrix composites (MMCs) with magnesium as the matrix material are promising alternatives to aluminum MMCs and heavy, conventional structural metals such as cast iron and stainless steels. For this reason, encouraging attempts are being made to incorporate these high-strength, lightweight materials in vehicles to save weight and thereby reduce deleterious vehicle emissions [10, 11]. In recent years, CNTs have been incorporated into Mg matrices in hopes to combine and refine the best properties of both constituents for an ideal material for just this purpose [12].

Since their discovery in 1991 by Iijima [13], CNTs have attracted researchers with their amazing aspect ratio and unparalleled electrical and thermal properties. Not only are CNTs a subject of great interest on their own, but also they offer themselves as excellent reinforcements to Mg MMCs as previous studies by a Swiss research group have indicated that the addition of 2 wt% CNT increases the elastic modulus of Mg by about 9% [14]. Another study reported a simultaneous improvement in both strength and ductility of Mg with the addition of 1.3 wt% CNT [15]. A number of researchers at the National University of Singapore studied the corrosion properties of Mg-CNT nanocomposites and their findings show that corrosion rate increases substantially with the presence of CNTs in the Mg matrix [16]. While these studies show that an improvement in *some* material properties can be obtained when CNTs are added to Mg, no attempts have yet been made to study the creep properties of these Mg nanocomposites.

In the present study, monolithic Mg along with Mg reinforced with 0.25, 0.5, and 0.75 vol% of CNTs are investigated for their creep and hardness responses. The creep properties of these materials are obtained through a

nanindentation (NI) technique, as opposed to conventional uniaxial testing. Nanindentation offers noteworthy advantages over uniaxial tension testing, for example: (1) indentation tests can be done to gather creep properties of individual constituents of a material system, i.e., a thin film or a single phase of a complex alloy; whereas uniaxial testing will only give an average creep property of the entire material, (2) uniaxial tests are time-consuming and indentation is quicker by comparison, (3) uniaxial tests need relatively large samples whereas a specimen with a volume of a cubic centimeter could be indentation-tested one hundred times, making much more use of the material area, and (4) indentation tests are considered to be non- or semi-destructive whereas uniaxial tests are destructive [17].

Indentation-based studies have been used by some researchers to shed light on magnesium's complex creep response. For example, Somekawa and Schuh [18] and Haghshenas et al. [19] used nano- and micro-indentation tests at high (150 s^{-1}) and low (10^{-5} – 10^{-1} s^{-1}) strain rates, respectively, to investigate the creep response of pure Mg at room and elevated temperatures. Through activation energy calculations, the studies have attributed dislocation slip and twinning to be the two dominant mechanisms controlling indentation creep of pure Mg. Haghshenas et al. [19] in particular, showed that these deformation mechanisms are operative and dominant over not only the aforementioned wide strain rate range, but also across a wide temperature range (295–573 K). Despite the well-documented creep behavior of pure Mg, the creep response and deformation mechanisms behind Mg-CNT nanocomposites remain a virgin field. For these reasons, indentation-based testing is used in this study to assess the complex and untouched field that is the creep behavior of the novel Mg-CNT nanocomposites at room temperature.

2 Experimental procedure

Magnesium powder was used as the matrix material, and high-purity (> 95%), single-walled carbon nanotubes (US Research Nanomaterials Inc.), 15–50 μm in length, with an average diameter of 1.1 nm were used as the reinforcement material in this study.

The powder metallurgy technique was used to fabricate both monolithic magnesium and magnesium-CNT nanocomposites containing 0.25, 0.5, and 0.75 vol% CNTs at the National University of Singapore. Correct amounts of Mg powders and their respective volume percentages of carbon nanotubes were carefully weighed and blended in absence of balls using a RETSCH PM-400 (Retsch GmbH, Haan, Germany) mechanical alloying machine at 200 rpm

for 2 h. The blended powders were compacted using a 100-ton uniaxial compaction machine to obtain a green compact. The green compact was then sintered using a hybrid microwave setup (640 °C for the total duration of approximately 15 min) to obtain a near-dense billet. The as-sintered billet was soaked at 400 °C for 1 h in a constant-temperature furnace prior to extrusion at 350 °C at an extrusion ratio of 20.25: 1 using a 150 T hydraulic press. Cylindrical rods of 8 mm diameter were obtained. The samples from the extruded rods were characterized for microstructure and properties. To ensure homogeneous microstructure and that the CNTs are distributed evenly in the structure and minimal clusters are present, characterizations were performed using a FE-SEM at high magnification. We have also selected an optimized extrusion ratio of 20.25:1. With this ratio, our porosity levels are less than 1% in most cases. To clarify, the properties discussed in this paper refer to those taken with measurements parallel to the extrusion direction. Further studies need to be performed in order to quantify the differences in properties.

Prior to characterizing the samples with optical microscopy and SEM, the samples were mounted in black phenolic mounting powder, the surface of each sample was mechanically polished with a series of progressively finer SiC sandpapers until each surface was mirror-like and scratch-free, and finally the samples were treated with a suspension of 0.1 μm alumina polishing powder, followed by a final polishing with bare cloth under water for approximately 10 min to remove any residual strains. Lastly, the samples were chemically treated in an acetic picric etchant (100 mL ethanol, 2.5 g picric acid, 25 mL acetic acid, and 25 mL water) for approximately 10 s to reveal microstructural characteristics.

The room temperature indentation creep tests were performed using an iNano Nanoindenter (Nanomechanics, Inc.) equipped with a diamond Berkovich indenter (tip roundness ≈ 100 nm). A constant loading rate followed by a constant load-hold scheme was used to study the time-dependent plastic deformation. During the testing, each sample is loaded at various strain rates of 0.01, 0.1, 1, and 10/s until a peak load of 50 mN is reached. The indentation load was then held constant for 500 s during which the plastic deformation (creep) data is recorded at fixed intervals. The indenter is then unloaded 10% of the maximum load and held for another 120 s for thermal drift correction to keep it below 0.05 nm/s. Indeed, the effect of thermal drift is negligible in this study as (i) tests were done at room temperature, and (ii) the dwell time is fairly short, 120 s.

The following section addresses the mathematical background necessary to assess the rate-dependent deformation response of the nanocomposite used in the present study via nanoindentation testing.

3 Steady-state creep theory for nanoindentation

The creep rate of crystalline material can be written as [20–24]:

$$\dot{\epsilon}_{\text{creep}} = \frac{AD_0Gb}{kT} \left(\frac{b}{d}\right)^p \left(\frac{\sigma}{\mu}\right)^n \exp\left(-\frac{\Delta Q}{kT}\right) \quad (1)$$

where σ is the applied stress, A is a coefficient related to temperature and microstructure, D_0 is the diffusion coefficient, G is the shear modulus, ΔQ is the activation energy for thermal-activated process, n is the stress exponent, p is the grain size exponent, k is the Boltzmann constant, T is the temperature, b is the Burgers vector and d is the grain size.

It is well documented that in conventional creep testing (i.e., uniaxial tension testing) creep deformation is negligible in most metallic materials at ambient temperature. However, this is not necessarily the case in the depth-sensing indentation testing. Here, triaxial stresses are developed underneath the indenter which can easily exceed the yield strength of the material even at low temperatures. To this end, Eq. 1 is reduced to the following equation for steady-state indentation creep:

$$\dot{\epsilon}_{\text{ind. creep}} = \frac{1}{h} \frac{dh}{dt} = B\sigma_{\text{ind}}^n \quad (2)$$

here, $\dot{\epsilon}_{\text{ind}}$ is the indentation strain rate (creep rate), B is a constant, n is the creep exponent, and σ_{ind} is the indentation stress.

It is also necessary to express indentation stress appropriately for a Berkovich pyramidal indenter tip [25]:

$$\sigma_{\text{ind}} = \frac{P}{24.56(h + 0.06R)^2} \quad (3)$$

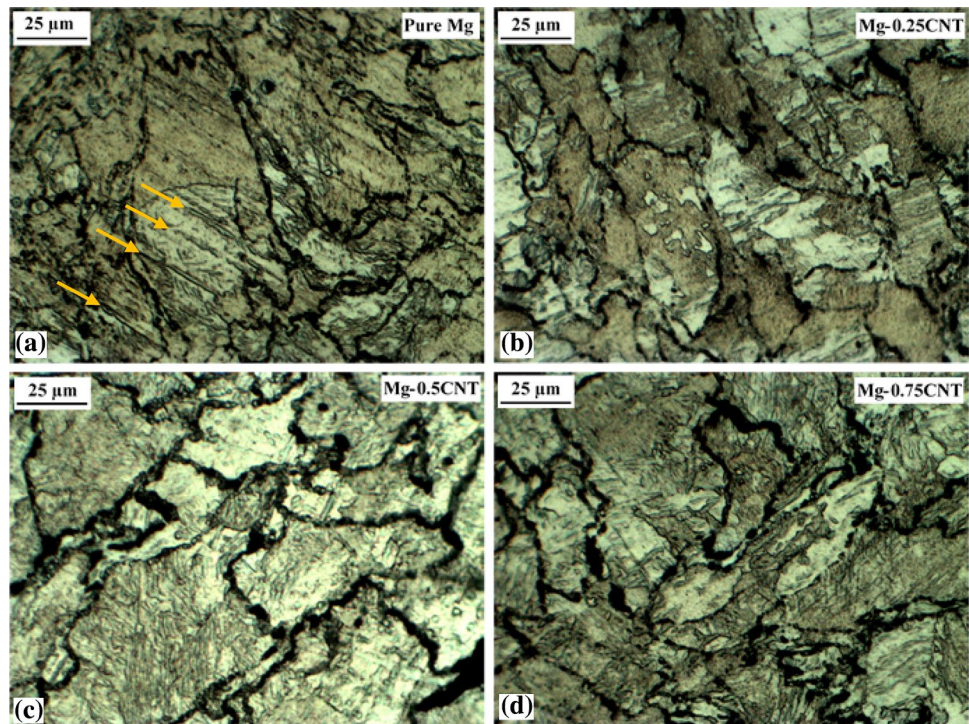
where h is instantaneous indentation depth and R is the indenter tip radius; i.e., 100 nm in this study.

A simple algebraic manipulation of Eq. 2 yields the following expression for n , the creep exponent:

$$n = \frac{\partial \ln \sigma_{\text{ind}}}{\partial \ln \dot{\epsilon}_{\text{ind}}} \quad (4)$$

By Eq. 4, the creep exponent is equal to the slope of a log–log plot of indentation stress versus indentation strain. This is the method that was used to determine n in the present study. The creep exponent is a useful quantity in determining what creep mechanism is dominant during depth-sensing experiments.

Fig. 1 Optical micrographs revealing the cross-sectional grain morphologies of **a** Pure Mg, **b** Mg-0.25 v/v% CNT, **c** Mg-0.5 v/v% CNT, and **d** Mg-0.75 v/v% CNT. Arrows are added to **a** to show the mechanical twins present in pure Mg



4 Results and discussion

4.1 Microstructure and grain morphology

Figure 1 shows the optical micrographs of the pure Mg and the Mg-CNT nanocomposites. Severely deformed grains, due to the hot extrusion operation in the manufacturing steps, are observed in the microstructure. Evidence of mechanical twins is also visible within the grains. Scanning electron microscopy (SEM) was also used to assess the integrity of the reinforcement-matrix interface. Evidence of the CNT is visible in high-magnification SEM images of the Mg-0.75 CNT nanocomposite, as shown in Fig. 2. Due to the method of fabrication of these samples, i.e., powder metallurgy, magnesium oxide particles tend to form during the processing. Some evidence of Mg oxides, detected with energy-dispersive spectroscopy (EDS) are shown in Fig. 3. The spectrum points 1, 2, 3, and 6 contain varying amounts of oxygen in addition to the Mg. Spectrum points 4 and 5 verify that the matrix material is indeed pure Mg as these points came up as 100% Mg as indicated in the table accompanying Fig. 3. It is expected that through addition of the CNTs to the Mg matrix some strain fields are developed which can enhance the dynamic recrystallization during the hot extrusion process. Also, the added CNTs can distribute on the grain boundaries and pin them. This then restricts grain boundary migration which may occur in the sintering and the extrusion processes. Having said

this, in our optical microscopy images we could see some marginal grain refinement in the Mg-CNT nanocomposites as compared with the pure Mg. This can be attributed to insufficient restriction ability of fine and individual CNTs to refine the grains. This is in agreement with the previous finding which indicated that a sufficient amount of nanoparticles at the grain boundary is needed for effective grain refinement [44]. Based on the OM images and the measurements the average grain size of the samples is measured as 75–100 μm .

4.2 Indentation results

4.2.1 Indentation load and indentation stress versus depth

The load–displacement curves for the Mg/CNT nanocomposite materials at room temperature are shown in Fig. 4. In the P – h curves of the studied materials, with an increase in the strain rate, the required load to reach a constant depth increases (work hardening effect). With an increase in the strain rate in the loading stage, the rate of dislocation generation and dislocation multiplication enhances [26–28].

These dislocations then are blocked by either the grain boundaries or the CNTs in the matrix. This confirms that the materials are rate sensitive at room temperature. This trend becomes more pronounced when the volume fraction of the CNTs increases simply because of the presence of more obstacles against dislocation motion.

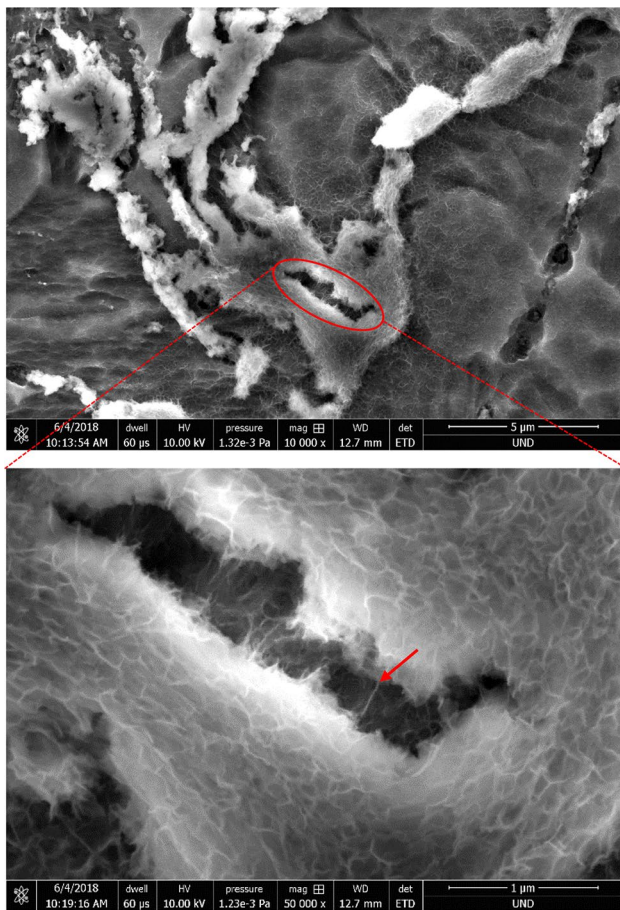


Fig. 2 Scanning electron microscopy (SEM) images of Mg-0.5 v/v% CNT. The higher-magnification image reveals an individual CNT fiber, indicated with an arrow

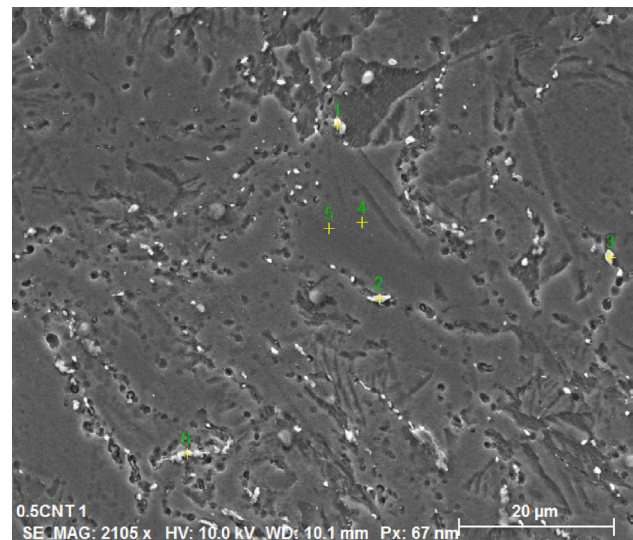
It is worth mentioning that the interface between the CNT and the Mg matrix is a potential place for nucleation and emission of the dislocations. This is mainly due to the difference in coefficient of thermal expansion between Mg and CNTs.

The hardening due to the thermal mismatch can be expressed as [29]:

$$\Delta\sigma_{\text{Thermal}} = \alpha G_m b \sqrt{\rho} \tag{5}$$

where α is a geometric constant and ρ is the dislocation density.

For the highest strain rate (10/s), it takes 5 s to reach the peak load of 50 mN; this number is 5×10^3 s for the slowest (0.01/s) strain rate. That is, for the case of fastest strain rate, the plastic deformation is “arrested” in the loading portion and then released in the constant load-hold (dwell) stage, which results in a pronounced creep displacement. On the other side, when the strain rate is low, most of the plastic deformation is “consumed” in the loading stage and that



Norm. mass percent (%)			
Spectrum	C	O	Mg
1	-	43.34	56.66
2	-	39.19	60.81
3	8.46	41.82	49.72
4	-	-	100.00
5	-	-	100.00
6	4.28	17.78	77.94

Fig. 3 Energy-dispersive X-ray spectroscopy (EDS) performed on Mg-0.5 v/v% CNT sample for confirmation of sample composition

results in less plastic deformation (creep) in the constant load-holding stage.

The phenomenon of indentation size effect (ISE) is a deviation from what is expected in classical plasticity. Specifically, in classical plasticity, hardness is constant no matter how deep or shallow the indent is. However, in-depth-sensing tests on the scale of nanometers, indentation size effects are observed in that hardness is higher at shallow indentations. Figure 5 contains evidence of this phenomenon. The ISE can be explained through dislocation starved plasticity (DSP) and strain gradient plasticity (SGP) [30–33].

According to the DSP, at the very early stage of the nanoindentation, the volume of the material beneath the indenter is extremely small which can be considered as dislocation-free structure [30]. Therefore, the strength of the material can be as large as the theoretical strength. When the indenter further moves within the sample, a larger volume of material is affected, additional space will be available for dislocations to generate. The SGP can be employed to explain the ISE. Here, to accommodate the shape of the indenter within the sample, geometrically necessary dislocations (GNDs) form underneath the indenter. Since there is still a limited space for the GNDs to generate and

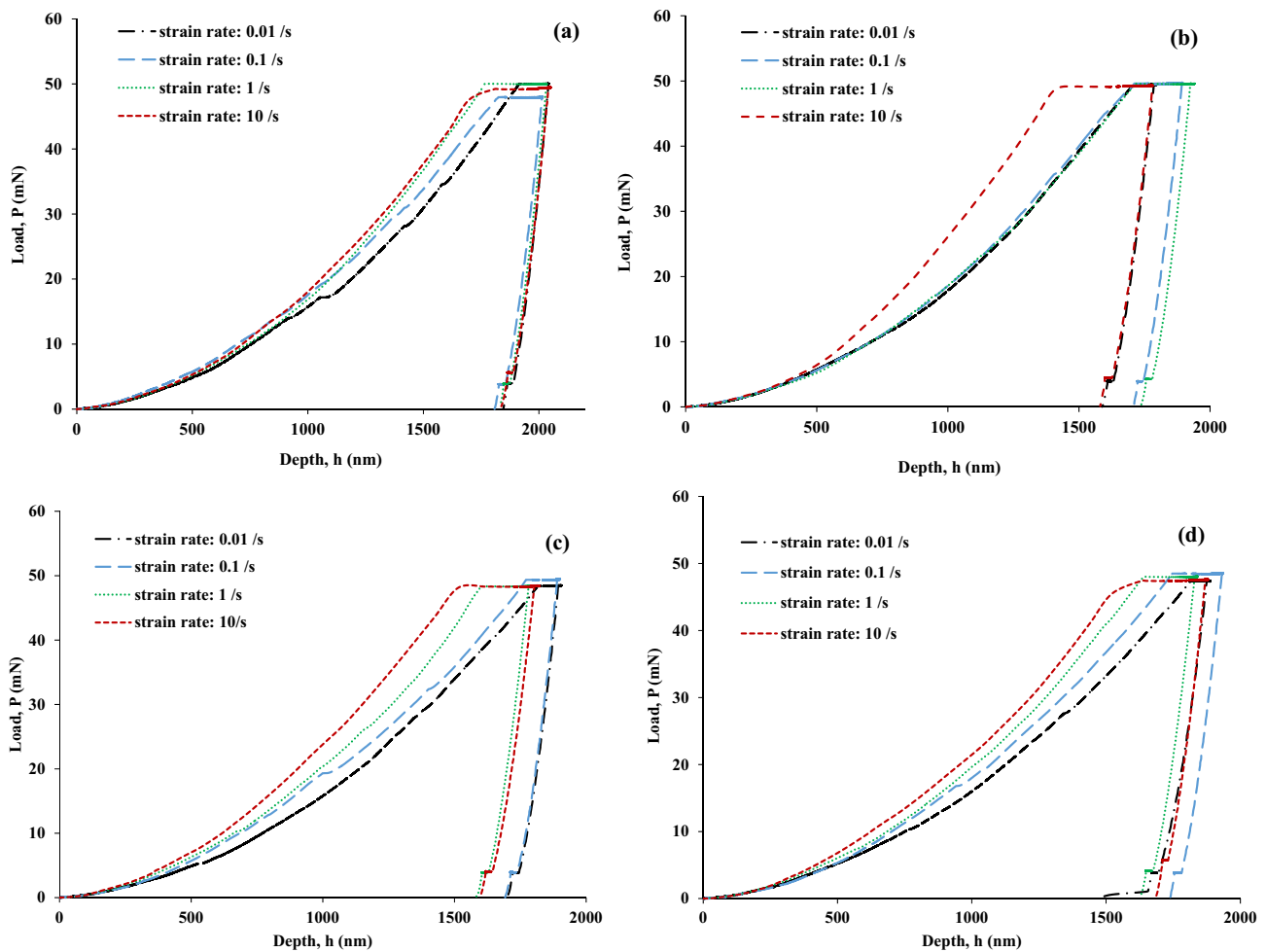


Fig. 4 Load–displacement curves displaying loading, holding, and unloading portions at different strain rates (0.01–10/s) for: **a** Pure Mg, **b** Mg-0.25 vol% CNT, **c** Mg-0.5 vol% CNT, and **d** Mg-0.75 vol% CNT. *Mg* Magnesium, *CNT* Carbon nanotube

interact, their Burger’s vector, mobility and slip systems are necessarily disparate compared with ordinary, statistically stored dislocations, SSDs. Therefore, the GNDs can directly contribute toward strengthening of the material in the shallow (near the surface) regions. It is observed that the ISE is more pronounced in the nanocomposite materials with a larger volume fraction of the CNTs. Here, when the volume fraction of the CNTs increases, the statistical number of the obstacles against dislocation (GNDs and SSDs) motion enhances. This produces a greater pile-up effect due to a stronger pinning effect of the obstacles (i.e., CNTs and/or grain boundaries). This creates a larger local work hardening effect through the Orowan strengthening effect [34]. The Orowan strengthening effect is given by [35, 36]:

$$\Delta\sigma_{\text{Orowan}} = \frac{0.8MG_m b}{\sqrt{\frac{\pi d^2}{2v_{\text{CNT}}}}} \tag{6}$$

where G_m is the shear modulus of the matrix; b is the value of the Burgers vector of the matrix; M is the Taylor factor; d is the diameter of the CNTs, and v_{CNT} is the volume fraction of the CNTs. However, when the indenter is well below the surface, large depth, there will be a balance between work hardening, induced by dislocation generation and multiplication, and dynamic recovery, induced by dilation rearrangement and annihilation. This results in a plateaued trend in the stress/depth curves for the large depths.

4.2.2 Indentation hardness as a function of CNT content

Hardness as a function of CNT content is also a trend of interest as it may seem counterintuitive initially that hardness decreases if CNT content is too high. Simply, CNTs have a tendency to agglomerate at high volume percentages due to van der Waals forces. This is the phenomenon that is attributed to the trends observed in Fig. 6. It can be seen that, overall, hardness begins to drop off at about

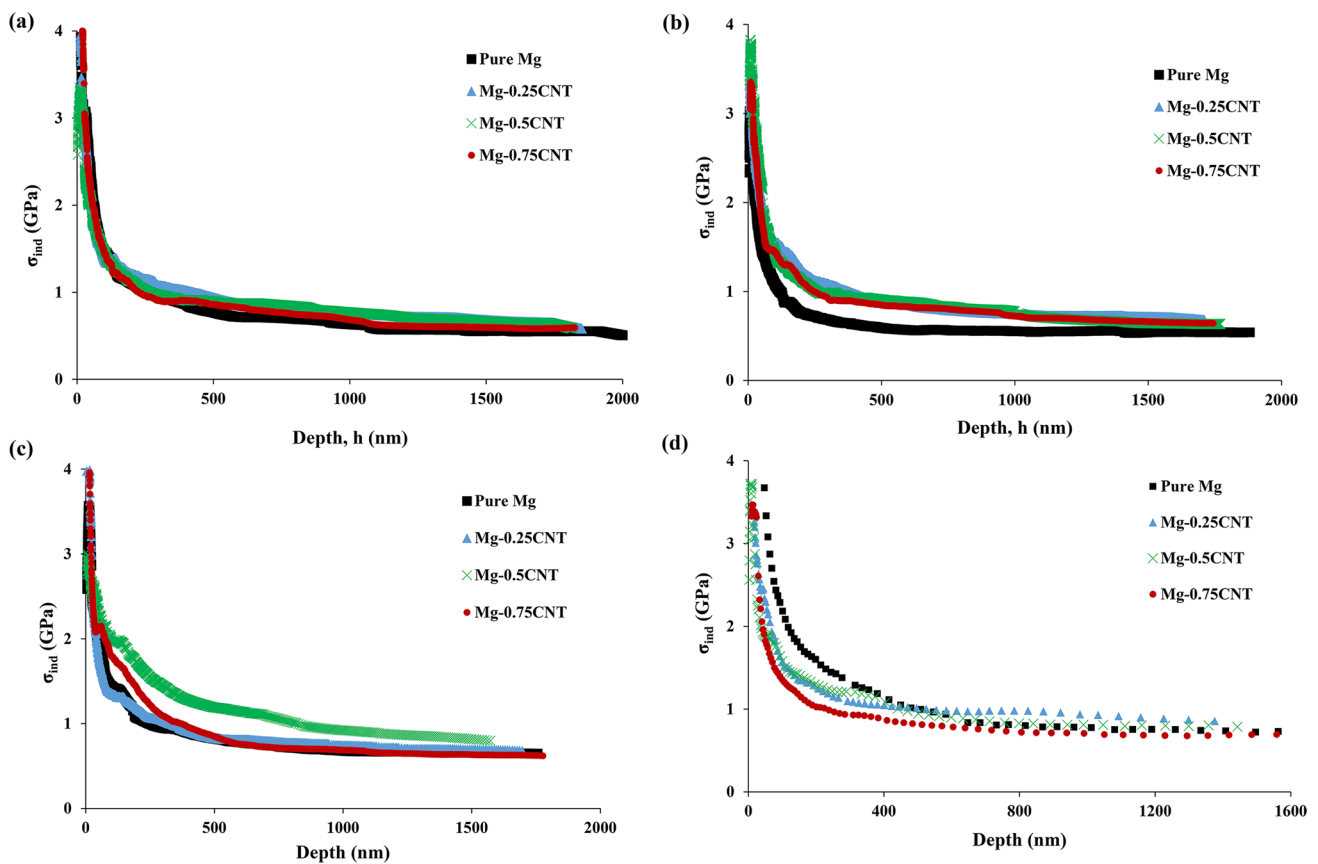


Fig. 5 Indentation stress versus displacement curve for the strain rate of: **a** 0.01/s, **b** 0.1/s, **c** 1.0/s, and **d** 10/s. The Indentation Size Effect (ISE) phenomenon is observed in all tests. *Mg* Magnesium; *CNT* Carbon nanotube; ISE: indentation size effect

0.5 vol% CNTs. This confirms that 0.5 vol% CNT seems to be an optimal volume fraction in the fabricated Mg-CNT materials.

However, as lower levels of CNT are added, the initially increasing trend in the microhardness for the nanocomposite samples can be attributed to (i) presence of harder CNTs in the matrix, (ii) the dispersion hardening effect of CNTs in the Mg matrix, (iii) strengthening effect caused by the presence of CNTs hindering the movement of the dislocation (suppressing the recrystallization and growth of crystal grains), (iv) effective load transfer from soft matrix onto the hard reinforcements owing to the superior interfacial bonding between the matrix and the reinforcement, and (v) generation of dislocations (mismatch in elastic modulus and CTE between Mg and CNTs) [37, 38].

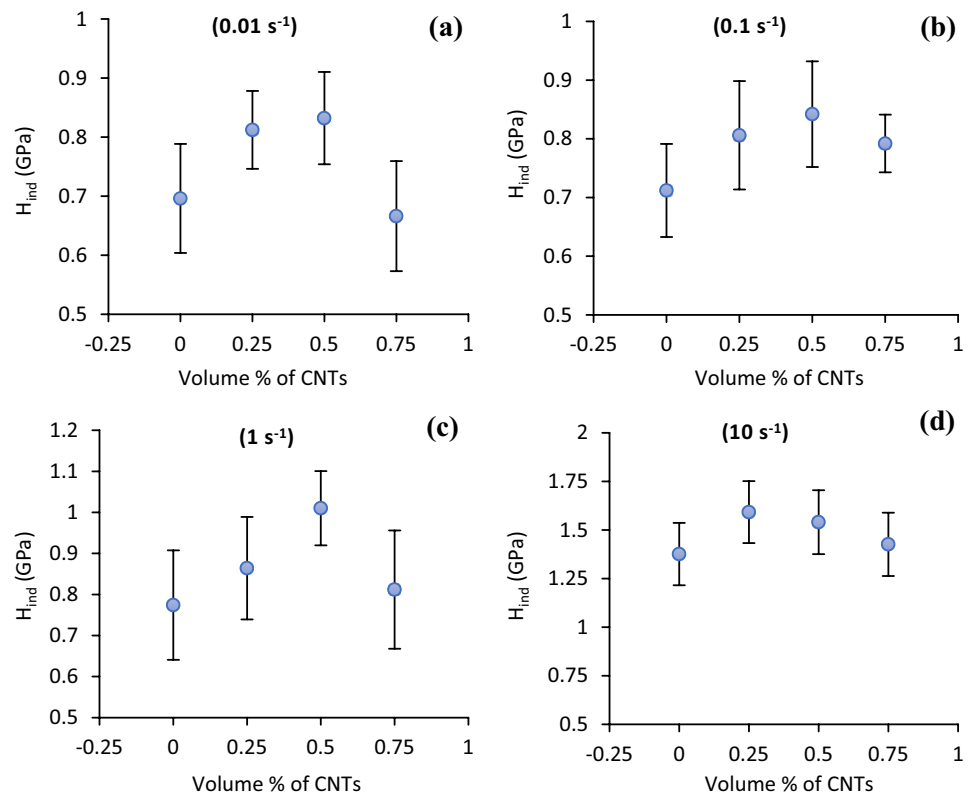
It is worth noting that the trend observed in Fig. 6 for the strain rate of 10 s^{-1} is slightly different than the others as hardness decreases after 0.25 vol% CNT, and not 0.5 vol% CNT. Note that each point on every graph in Fig. 6 is representative of 5 trials and that these tests were done on “nano” scale. This means that it is nearly impossible to tell what region of the material was indented as the tip could have been on a grain boundary, a grain, a CNT-dense

area, a magnesium oxide area, an area of pure Mg, etc. The overall trend is that hardness has been observed to be at its highest at intermediate volume percentages of CNTs.

4.2.3 Creep rate as a function of time

Creep is temperature—and time-dependent deformation under a constant load. Therefore, in the constant strain rate, constant load-hold indentation scheme, the dwell period is where the creep is expected. Dwell time in this study is 500 s at a constant load of 50 mN. It is worth mentioning that the indentation creep test being of compressive nature does not demonstrate any tertiary stage. In the absence of a tertiary stage, the steady-state stage provides a stable zone underneath the indenter. It is worth mentioning that it should be noted that in the nanoindentation creep the stress state underneath the indenter is a local and triaxial stress. Besides, stress distribution in the depth-sensing indentation technique is much more complex than uniaxial tensile/compressive creep tests, and at low displacement the maximum shear stress beneath the indenter exceeds the yield stress of the specimen (large triaxial stresses in the range of a few gigapascals).

Fig. 6 Variation of indentation hardness as a function of CNT loading over four strain rates: **a** 0.01 s^{-1} , **b** 0.1 s^{-1} , **c** 1 s^{-1} , and **d** 10 s^{-1}



This phenomenon causes the occurrence of creep in the materials, at ambient (room) temperatures and over a short period of time contrasting traditional creep tests which show creep mainly at elevated temperatures over an extended time period.

The triaxial stress state induced in the nanoindentation tests is quite complex and completely different with what is produced in the uniaxial creep tests. This may lead to some errors and inaccuracies (i.e., surface effects, indentation size effect, etc.) associated with the indentation creep approach.

There are intrinsic differences in the deformation mechanics in the indentation and the uniaxial creep:

- i. The stress state beneath the indenter is relatively localized and is much more complicated than that in uniaxial tests.
- ii. The loading rate during the indentation is 2–3 magnitudes faster than conventional creep tests, and the recovery process for the deformation can be retarded.
- iii. Due to the stability of the indentation instruments, limited creep duration and temperatures can be performed.

Figures 7 and 8 show the observed trends in creep displacement and creep rate over the 500 s dwell period,

respectively. The vertical lines in Fig. 7 distinguish the transition in creep stage, as the creep displacement curves to the left are representative of primary creep and to the right of the line, the creep is approximately steady state. Since it is of interest to identify the mechanisms responsible for creep at room temperature in these samples, the steady-state curves in Fig. 7 will be analyzed in isolation from the primary creep portions. This is because the creep power law that will be employed is only valid for the steady-state creep.

As observed, pure Mg shows the highest creep rate of all the samples tested. These observations overall support that CNTs do contribute to the creep resistance of magnesium either through pinning the grain boundaries or blocking dislocations glide. The plastic deformation, i.e., creep, in a crystalline material generally takes place by the generation and movement of dislocations along the slip planes. However, the presence of nanosize reinforcement (i.e., CNTs in this study) can act as effective obstacles to the dislocations movement and impede their motion. Furthermore, the piled-up dislocations provide a back-stress that oppose the applied stress in a creep test. These effects are however absent in the case of pure Mg and that is why the creep rate is higher in pure Mg as compared with the Mg-CNT nanocomposites. That is, the presence of the dislocation pile-ups around the grain boundaries and/or nanosize reinforcements

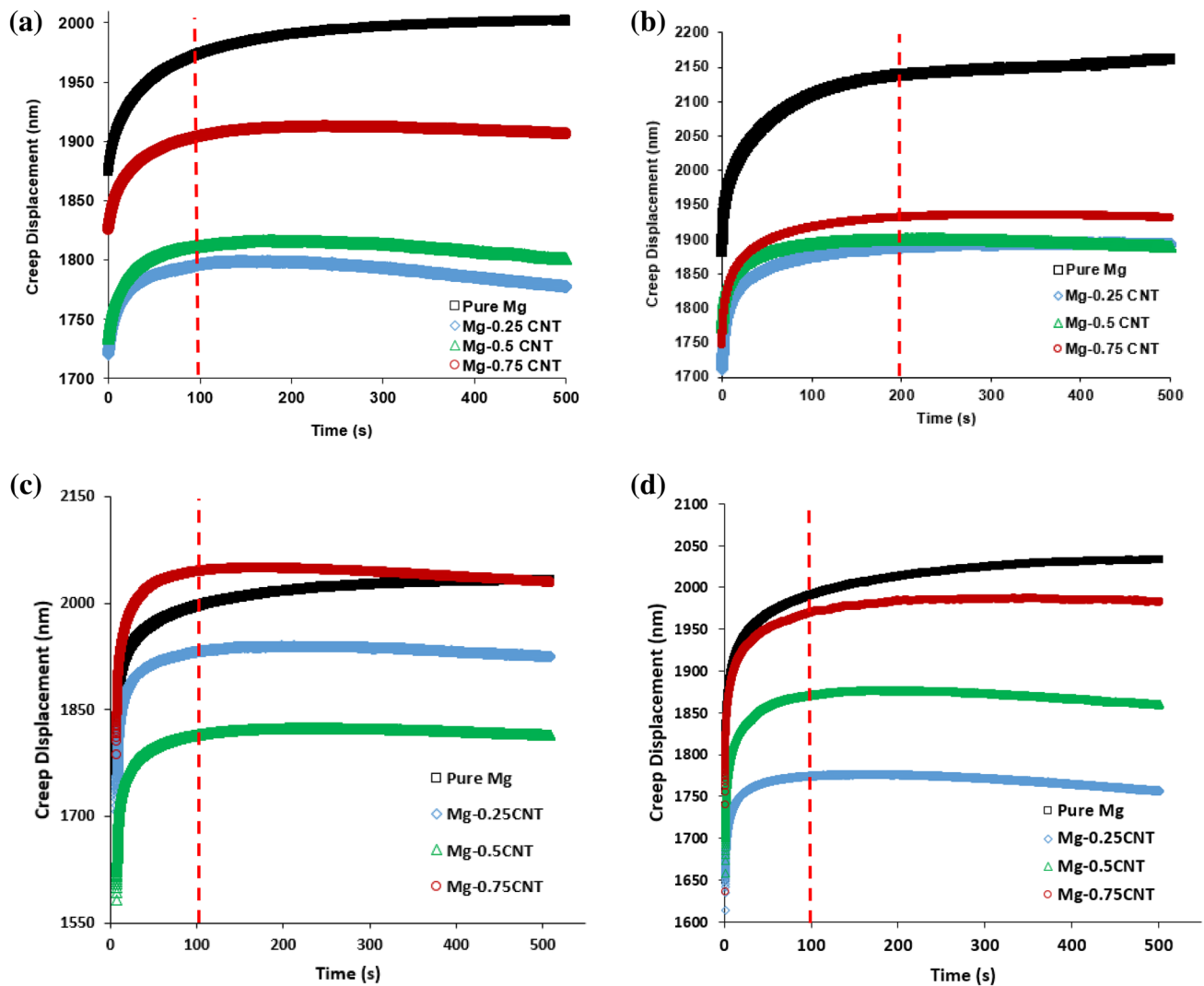


Fig. 7 Creep displacement and creep rate versus hold time (500 s) for pure Mg and Mg-CNT nanocomposites at four distinct strain rates: **a** 0.01/s, **b** 0.1/s, **c** 1.0/s, and **d** 10/s. Transient and steady-state creep are observed in all curves. *Mg* Magnesium; *CNT* Carbon nanotube

along with the dislocation tangles, due to dislocation/dislocation interaction, resulted in the work hardening effect at room temperature, which leads to enhanced creep resistance of the nanocomposites.

To assess what creep deformation mechanism dominates at room temperature for this material, Eq. 4 will be used to assess what the creep exponent is for each trial performed. The magnitude of n is the parameter of interest, as it will indicate the creep mechanism at work. When $n=1$, Nabarro-Herring Creep (Coble Creep) is the dominant creep mechanism, which is a diffusional creep mechanism. If $n=2$, grain boundary sliding is the mechanism responsible for creep. Finally, if n is three or greater, the creep is attributed to dislocation movements (dislocation creep) [39–42]. Figure 9 shows the creep exponents obtained through Eq. 4 for various materials studied in the present

paper versus the employed indentation strain rates. The value of n is greater than three in every trial. From this, it is safe to conclude that dislocation creep, by glide of dislocations in their slip planes, is the dominant mechanism of cold flow (creep at room temperature) in the Mg-CNT nanocomposites studied in this research. The largest n -values belong to the Mg-0.5 vol% CNT nanocomposite sample which, according to Fig. 6, possesses the highest hardness. Therefore, it seems the optimum percentage of CNT content, which provides the best creep resistance, in this study, is Mg-0.5 vol% CNT nanocomposite. When the CNT content is increased to 0.75 vol%, both hardness and creep resistance drop. This can possibly be attributed to the CNT clustering (agglomeration) effect and non-uniform distribution of the clusters, now in micron sizes, in the Mg matrix. With an increase in the volume fraction of

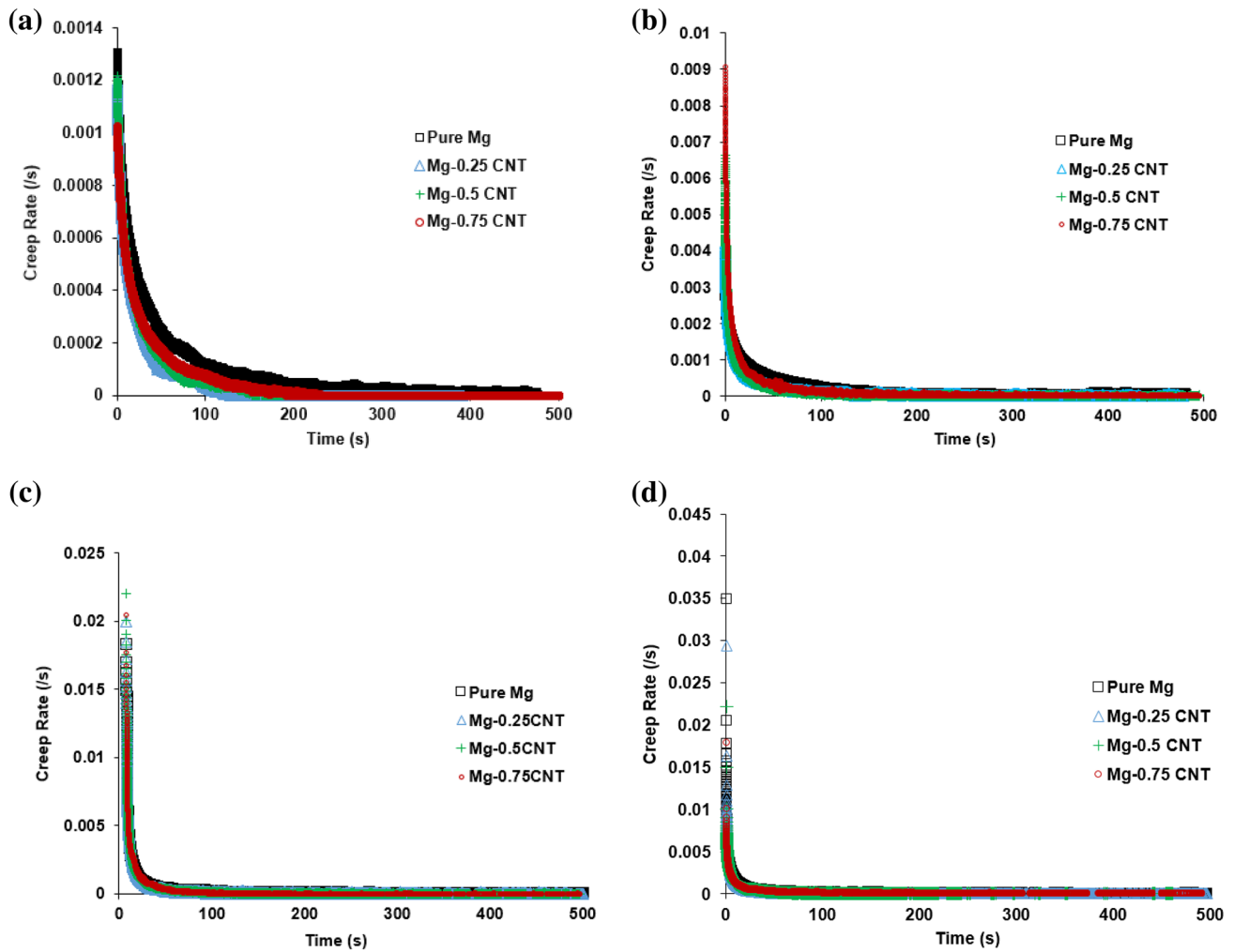


Fig. 8 Creep rate versus hold time (500 s) for all four samples at the four strain rates: **a** 0.01/s, **b** 0.1/s, **c**, 1.0/s, and **d** 10/s

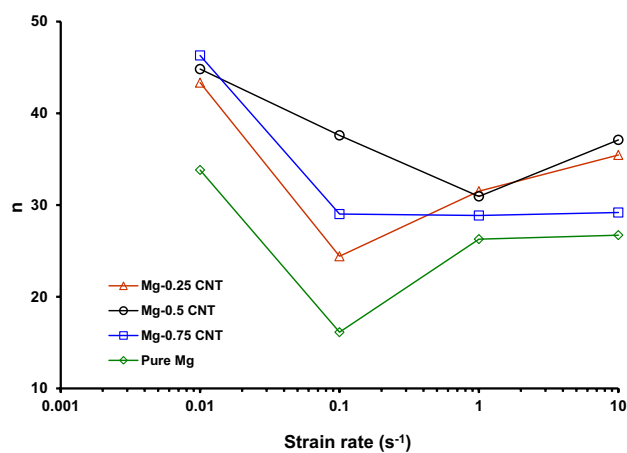


Fig. 9 Creep stress exponent (n) values for all strain rates tested

the CNT, the nanotubes, due to the large Van der Waals effect, are merged and coarsened and lose their effective contribution toward the strengthening of the Mg matrix. Similar creep behavior has been reported in Al reinforced with nanoparticles, which has also been attributed to the Orowan strengthening mechanism mentioned earlier [43].

In the holding stage, it is observed that creep rate tends to decrease with increasing depth. This trend is exhibited in Fig. 10. It is clear from this figure that higher creep rates are observed at shallower depths in the sample. It also appears that creep rate decreases constantly for a portion of the holding time, and then levels off.

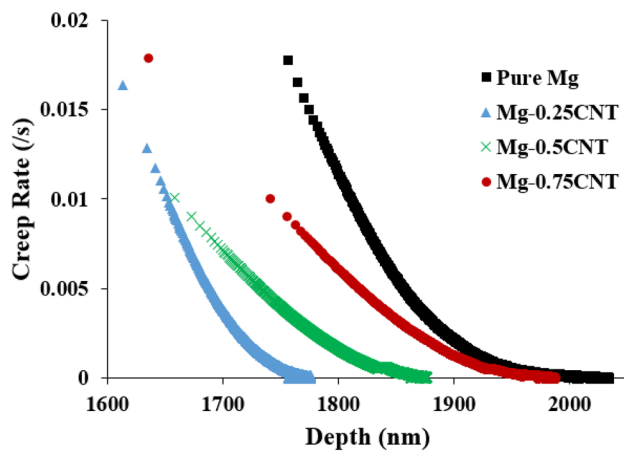


Fig. 10 Creep rate versus indentation depth for pure magnesium and the Mg-CNT nanocomposites at the strain rate of 10/s

5 Conclusions

This study explored the ambient temperature time-dependent plastic deformation of a family of Mg-CNT nanocomposites through a method of instrumented nanoindentation testing. The following conclusions are drawn:

1. Carbon nanotubes improve both strength and the creep resistance of the Mg matrix.
2. Hardness reaches its highest value at intermediate volume percentages of CNTs, equal to 0.5 vol% in the present study.
3. With an increase in the volume fraction of the CNTs beyond 0.5%, hardness and creep resistance decrease due to CNT agglomeration.
4. The ambient temperature creep mechanism of the studied Mg-CNT nanocomposites and the matrix material (pure Mg) is considered to be dislocation controlled creep via dislocation glide.
5. Results of this paper can be used as a baseline to study high-temperature creep behavior of the Mg-CNT nanocomposites to determine what deformation mechanisms are operated at elevated temperatures.

Acknowledgements This work has been financially supported by the National Science Foundation (NSF) under Grant #1458962.

Compliance with ethical standards

Conflict of interest The authors declare that they have no conflict of interest.

References

1. Mordike BL, Friedrich HE (2006) Magnesium technology: metallurgy, design data, applications. Springer, Berlin, p 257
2. Gupta M, Sharon NML (2011) Magnesium, magnesium alloys, and magnesium composites. Wiley-blackwell, Hoboken, pp 5–11
3. Hu XS, Zhang YK, Zheng MY, Wu K (2005) A study of damping capacities in pure Mg and Mg-Ni alloys. *Scripta Mater* 52:1141
4. Lei W, Wang T, Wang H, Liang W (2018) Microstructure and mechanical properties of pure magnesium subjected to hot extrusion. Review article. *Adv Mater Sci Eng* 2:1–3
5. Mathaudhu SN, Luo AA, Neelameggham NR, Nyberg EA, Sillekens WH (2014) Essential readings in magnesium technology. Wiley, Hoboken, p 298
6. Mo N, Tan Q, Bermingham M, Huang Y, Dieringa H, Hort N, Zhang M (2018) Current development of creep-resistant magnesium cast alloys: a review. *Mater Design* 155:422
7. Haghshenas M, Wang Y, Cheng Y-T, Gupta M (2018) Indentation-based rate-dependent plastic deformation of polycrystalline magnesium. *Mater Sci Eng, A* 716:63
8. Paramsothy M, Chan J, Kwok R, Gupta M (2011) Addition of CNTs to enhance tensile/compressive response of magnesium alloy ZK60A. *Compos Part A* 42:180–188
9. Dieringa H (2011) Properties of magnesium alloys reinforced with nanoparticles and carbon nanotubes: a review. *J Mater Sci* 46:289–306
10. Ceschini L, Dahle A, Gupta M, Jarfors A, et al. (2017) Aluminum and magnesium metal matrix nanocomposites. Springer, Singapore, pp 1–2, pp 10–13
11. Dey A, Pandey M (2015) Magnesium metal matrix composites—a review. *Rev Adv Mater Sci* 42:58
12. Tjong SC (2013) Recent progress in the development and properties of novel metal matrix nanocomposites reinforced with carbon nanotubes and graphene nanosheets. *Mater Sci Eng, R* 74:282
13. Iijima S (1991) Helical microtubules of graphitic carbon. *Nature* 354:56–58
14. Swiss research group (2004) Tiny tubes boost for metal matrix composites. *Metal Powder Rep* 59:40–43. [https://doi.org/10.1016/S0026-0657\(04\)00207-3](https://doi.org/10.1016/S0026-0657(04)00207-3)
15. Goh CS, Wei J, Lee LC, Gupta M (2006) Simultaneous enhancement in strength and ductility by reinforcing magnesium with carbon nanotubes. *Mater Sci Eng, A* 423:153–156
16. Aung N, Zhou W, Goh C, Nai S, Wei J (2010) Effect of carbon nanotubes on corrosion of Mg-CNT composites. *Corros Sci* 52:1551–1553
17. LaManna JA Jr (2006) A study of the relationship between indentation creep and uniaxial creep. PhD diss. University of Tennessee, Knoxville
18. Somekawa H, Schuh CA (2012) High-strain-rate nanoindentation behavior of fine-grained magnesium alloys. *J Mater Res* 27:1295–1302
19. Haghshenas M, Bhakhri V, Oviasuyi R, Klassen RJ (2015) Effect of temperature and strain rate on the mechanisms of indentation deformation of magnesium. *MRS Commun* 5:513–518
20. Katsarou L, Mounib M, Lefebvre W, Vorozhtsov S, Pavese M, Badini C, Molina-Aldareguia JMM, Jimenez CC, Prado MTP, Dieringa H (2016) Microstructure, mechanical properties and creep of magnesium alloy Elektron21 reinforced with AlN nanoparticles by ultrasound-assisted stirring. *Mater Sci Eng, A* 659:84–92. <https://doi.org/10.1016/j.msea.2016.02.042>
21. Mukherjee AK, Bird JE, Dorn JE (1969) *Trans ASM* 62:155–179

22. Ganguly S, Mondal AK (2018) Influence of SiC nanoparticles addition on microstructure and creep behavior of squeeze-cast AZ91-Ca-Sb magnesium alloy. *Mater Sci Eng, A* 718:377–389
23. Fernández R, González-Doncel G (2008) Threshold stress and load partitioning during creep of metal matrix composites. *Acta Mater* 56:2549–2562
24. Ma ZY, Mishra RS, Tjong SC (2002) High-temperature creep behavior of TiC particulate reinforced Ti-6Al-4V alloy composite. *Acta Mater* 50:4293–4302
25. Muhammad M, Masoomi M, Torries B, Shamsaei N, Haghshenas M (2018) Depth-sensing time-dependent response of additively manufactured Ti-6Al-4V alloy. *Addit Manuf* 24:37–46
26. Khantha M, Vitek V, Pope DP (2001) Strain-rate dependent mechanism of cooperative dislocation generation: application to the brittle-ductile transition. *Mater Sci Eng, A* 319–321:484–489
27. Fan Y, Osetskiy YN, Yip S, Yildiz B (2013) Mapping strain rate dependence of dislocation-defect interactions by atomistic simulations. *Proc Nat Acad Sci U S A* 110(44):17756–17761
28. Gurrutxaga-Lerma B, Balint DS, Dini D, Sutton AP (2015) The mechanisms governing the activation of dislocation sources in aluminum at different strain rates. *J Mech Phys Solids* 84:273–292
29. Mizra FA, Chen DL (2015) A unified model for the prediction of yield strength in particulate-reinforced metal matrix nanocomposites. *Materials* 8(8):5138–5153
30. Elmustafa AA, Stone DS (2002) Nanoindentation and the indentation size effect: kinetics of deformation and strain gradient plasticity. *J Mech Phys Solids* 51:357–381
31. Zhao M, Slaughter WS, Li M, Mao SX (2003) Material-length-scale-controlled nanoindentation size effects due to strain-gradient plasticity. *Acta Mater* 51:4461–4469
32. Zhang X, Aifantis KE (2015) Interpreting the internal length scale in strain gradient plasticity. *Rev Adv Mater Sci* 41:72–83
33. Nix WD, Greer JR, Feng G, Lilleodden ET (2007) Deformation at the nanometer and micrometer scales: effects of strain gradients and dislocation starvation. *Thin Solid Films* 515:3152–3157
34. Hull D, Bacon DJ (2001) *Introduction to Dislocations*, 4th edn. Butterworth-Heinemann, Oxford
35. Li Q, Viereckl A, Rottmair CA, Singer RF (2009) Improved processing of carbon nanotube/magnesium alloy composites. *Compos Sci Technol* 69:1193–1199
36. Li CD, Wang XJ, Liu WQ, Shi HL, Ding C, Hu XS, Zheng MY (2014) Microstructure and strengthening mechanism of carbon nanotubes reinforced magnesium matrix composite. *Mater Sci Eng, A* 597:264–269
37. Zhou M, Xiaoni Q, Ren L, Fan L, Zhang Y, Guo Y, Quan G, Tang Q, Liu B, Sun H (2017) *Materials* 10(138):5. <https://doi.org/10.3390/ma10121385>
38. Li F, Xie Y, Song M, Ni S, Guo S, Liao X (2016) A detailed appraisal of the stress exponent used for characterizing creep behavior in metallic glasses. *Mater Sci Eng, A* 654:53–59
39. Sherby OD, Burke PM (1968) Mechanical behavior of crystalline solids at elevated temperature. *Prog Mater Sci* 13:325–389
40. Mohamed FA, Park KT, Lavernia EJ (1992) Creep behavior of discontinuous SiC-Al composites. *Mater Sci Eng, A* 150:21–35
41. Weertman J (1957) Steady state creep through dislocation climb. *J Appl Phys* 28(3):362–364
42. Weertman J (1957) Steady state creep of crystals. *Appl Phys* 28(4):1185–1189
43. Tjong SC, Ma ZY (1997) The high-temperature creep behavior of aluminum-matrix composites reinforced with SiC, Al₂O₃, and TiB₂ particles. *Compos Sci Technol* 57(6):697–702
44. Kang YC, Chan SL (2004) Tensile properties of nanometric Al₂O₃ particulate-reinforced aluminum matrix composites. *Mater Chem Phys* 85:438–443

Publisher's Note Springer Nature remains neutral with regard to jurisdictional claims in published maps and institutional affiliations.